Full Paper

Wiley Online Library

ELECTROANALYSIS

DOI: 10.1002/elan.201700789

Title Quartz-Crystal Microbalance Measurements of CD19 Antibody Immobilization on Gold Surface and Capturing B Lymphoblast Cells: Effect of Surface Functionalization

Kutay Icoz[+],*[a] Mehmet Cagri Soylu[+],[b] Zeynep Canikara,[b] and Ekrem Unal[c]

Abstract: We have investigated different surface functionalization methods to immobilize CD19 antibody on gold surface to capture B lymphoblast cells associated with the acute lymphoblastic leukemia disease. Quartz Crystal Microbalance measurements were performed to analyze the binding kinetics of each layer and determine the optimum method, which results in higher cell capture rates. The random orientation of antibody and oriented antibody through protein G was investigated and protein G presence resulted in 15,2 Hz frequency shift for 10^4 cells/mL. The 3-mercaptopropyltrimethoxysilane (MPS) and 11-Mercaptoundecanoic acid (MUA) coatings of gold surface together with 4-(N-Maleimidomethyl) cyclohexane-1-carboxylic acid 3-sulfo-N-hydroxysuccinimide ester sodium salt (Sulfo-SMCC) and N-Ethyl-N'-(3-dimethylaminopropyl) carbodiimide hydrochloride (EDC)/N-hydroxysulfosuccinimide (NHS) linker layers were tested on QCM for protein G and antibody binding. The results indicate that MUA, EDC/NHS, protein G, antibody CD19 is the optimum surface modification among the tested combinations. By using the optimum surface functionalization method, minimum 10^3 cell per mL was measured as 1.9 Hz frequency shift.

Keywords: surface functionalization · acute lymphoblastic leukemia · quartz crystal microbalance with dissipation · CD19 immobilization · B lymphoblast · protein G

1 Introduction

According to the American Cancer Society, Leukemia is the most common type of cancers in childhood. Even though some of the children with acute lymphoblastic leukemia achieve complete remission and no clinical symptoms are observed, leukemia may relapse know as Minimal Residuel Disease (MRD) [1–3]. There is a consensus on the necessity of MRD monitoring for increasing the treatment efficiency [2]. MRD is monitored using multicolored Flow cytometry and CD19, CD34 and CD10 antigens are determined as the backbone panel for MRD detection [3]. In order to develop a MRD biochip and capture leukemia cells on a sensor surface, immobilization of CD19 on gold surface has to be investigated. Immobilization of antibodies as receptors on the surfaces is of utmost importance for the performance of a biosensor. Antibodies recognize the analyte based on affinity and this recognition is transduced to another type of signal that can be measured [4]. Advancements in micro and nano technology revealed development of novel transducers such as cantilevers [5–7], nanowires [8–10], surface plasmon resonators (SPR) [11–13], microelectrodes [14–16] and micro/nano particles such as gold [17–19], silver [20–22] nanoparticles, and immunomagnetic beads [23–26]. Various methods have been reported for immobilizing antibodies on transducers [27–29] or micro/nano particles [30–32]. For gold surfaces, self–assembled monolayers of thiol group (–SH) or carboxyl group (–COOH) are dominantly preferred due to the formation of stable bonds [33]. Formation of a self-assembled monolayer of MUA and EDC/NHS activation of the carboxyl group of MUA layer was extensively used to immobilize antibodies on a gold surface for SPR based biosensing [34,35]. Another thiol group including coating agent is MPS that is able to easily undergo a hydrolysis and condensation process in aqueous ethanol solution at high pH. At appropriate conditions, those processes could be controlled to provide adequate electrical insulation, favorable surface morphology and chemistry for sensors used for bio-detection in ionic bio-fluids. The condensed layer of MPS on a piezoelectric sensor measuring binding surface stress induces detection resonance shift, and enables optimal binding on a structurally smooth surface [36].

It has been also shown that the antibody orientation on the transducer surface affects the capture efficiency of

[a] K. Icoz[+]
BioMINDS (Bio Micro/Nano Devices and Sensors) Lab, Department of Electrical and Electronics Engineering, Abdullah Gul University, 38080, Kayseri, Turkey
E-mail: kutay.icoz@agu.edu.tr
[b] M. C. Soylu,[+] Z. Canikara
Biomedical Engineering Department, Erciyes University, 38030, Kayseri, Turkey
[c] E. Unal
Division of Pediatric Hematology, Department of Pediatrics, Faculty of Medicine, Erciyes University, 38030, Kayseri, Turkey
[+] Authors contributed equally.

the target molecule [37,38]. One strategy of obtaining the oriented antibody is immobilizing antibodies on the surface so that antigen binding sites (Fab) are directed towards the analyte [39]. Protein G has binding sites for the constant Fc region of mammalian immunoglobulin Gs (IgGs) [40], and antibody immobilization on a preformed layer of protein G provided improved sensitivity compared to the antibody immobilization without protein G layer [41].

Quartz Crystal Microbalance (QCM) sensor is a nanogram sensitive technique that has been used in the wide range of bio-detection applications to detect various bio-analytes such as herbicide, virus, bacteria, DNA/RNA, protein, cell and tissue by using resonance frequency change due to total mass increment on gold coated quartz crystal surface [42–48]. QCM sensor has been extensively used for measuring antigen-antibody interactions [49–53]. Quartz Crystal Microbalance with Dissipation (QCM-D) monitoring enables real-time, label free measurements of molecular adsorption and/or interaction on crystal surface. Besides, it also enables to monitor the viscoelastic properties of adsorbed layer via dissipation parameter (D) patented by Q-Sense®. Dissipation takes place when the voltage on the crystal is shut off and the energy of oscillating crystal dissipates [54,55].

Sauerbrey Equation explaining linear relation between the changes in the resonance frequency of a quartz crystal and the mass change on its surface. The QCM's resonance frequency change, Δf, was related to the total mass change per unit area at the QCM surface, Δm, as;

$$\Delta m = -C.\ \Delta f/n \tag{1}$$

where f was the resonance frequency of the QCM, C was the sensitivity factor (17.7 $ng\,Hz^{-1}\,cm^{-2}$) [56,57], and n was the the overtone number ($n = 1, 3, 5, 7$).

This paper presents the QCM–D experiments of six different techniques to immobilize CD19 antibody on gold surface (Figure 1) to capture the B lymphoblast cells. In the next sections we detail the experimental procedure, present and discuss the results.

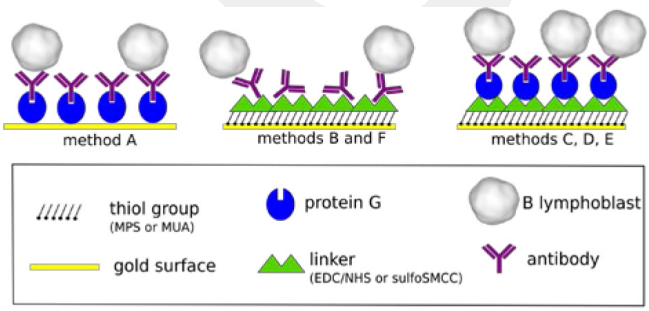

Fig. 1. Illustration of the tested surface modification methods (methods A, B, C, D, E and F) to capture B lymphoblast cells on a gold surface.

2 Materials and Methods

Direct Protein G adsorption on gold surface, MPS or MUA coatings with Sulfo-SMCC, EDC/NHS linkers and impact of protein G were experimentally tested (Table 1).

Table 1. Tested surface modification methods.

Methods	Thiol Group	Linker	Orientation Protein	Antibody
Method A	–	–	Protein G	CD19
Method B	MPS	Sulfo-SMCC	–	CD19
Method C	MPS	Sulfo-SMCC	Protein G	CD19
Method D	MUA	EDC/NHS	Protein G	CD19
Method E	MPS	EDC/NHS	Protein G	CD19
Method F	MPS	EDC/NHS	–	CD19

Method A relies on the adsorption of protein G on bare gold surface [58], without any pre-coating of the surface. The main steps of the immobilization procedure are (Bovine Serum Albumin (BSA)):

$$Gold \gg ProteinG \gg CD19 \gg BSA \gg Blymphoblast \tag{2}$$

Method B uses the formation of MPS self assembled monolayer on gold surface [36], then for activation of the surface Sulfo-SMCC linker layer was formed. The main steps of the immobilization procedure are:

$$Gold \gg MPS \gg Sulfo-SMCC \gg CD19 \gg BSA \gg Blymphoblastcells \tag{3}$$

Method C includes protein G on gold surface pre-modified with MPS and Sulfo-SMCC layers. The main steps of the immobilization procedure are:

$$Gold \gg MPS \gg Sulfo-SMCC \gg ProteinG \gg CD19 \gg BSA \gg Blymphoblastcells \tag{4}$$

Method D uses the formation of MUA self assembled monolayer and EDC/NHS, cross linking followed by protein G modification [59]. The main steps of the immobilization procedure are:

$$Gold \gg MUA \gg EDC/NHS \gg ProteinG \gg CD19 \gg BSA \gg Blymphoblastcells \tag{5}$$

Method E uses the combination of MPS coating and EDC/NHS linking. The methoxy groups on the free MPS molecules are hydrolyzed in the aqueous ethanol solution, as well as, the thiol groups on the MPSs are engaged on the gold surface of QCM via Thiol-Gold interaction. Due

to the high pH (pH = 9.0), hydroxyl groups on MPS molecules engaged on the surface commence to condense with the next engaged MPS molecule's hydroxyl group, and this condensation forms the tight MPS coating on the gold surface. After condensation, free nucleophilic hydroxyl groups remaining on the coating react with the electrophilic carbodiimides of EDC. The cross-linking binding of EDC/NHS produces amine reactive sensor surface, and provides the Protein Gs' amine groups to bind with the Sulfo-NHSs. The main steps of the immobilization procedure are:

$$Gold \gg MPS \gg EDC/NHS \gg ProteinG \gg CD19 \gg BSA \gg Blymphoblastcells \quad (6)$$

Method F is designed to investigate the impact of protein G. The steps in method E are exactly followed except the Protein G step. The main steps of the immobilization procedure are:

$$Gold \gg MPS \gg EDC/NHS \gg CD19 \gg BSA \gg Blymphoblastcells \quad (7)$$

By measuring the frequency shift after the B lymphoblast cell capture step on the QCM sensor, we determined the method with highest efficiency. Also the impact of BSA passivation layer to cell capture ratio for the method E was explored as a result of experimental observation.

2.1 Materials

CD19 antibody was purchased from Biolegend (San Diego, CA). Protein G was purchased from Thermo Scientific (Pittsburgh, PA). B lymphoblast cells CCRF-SB were purchased from ATCC (Rockville, MD), and all other chemicals were purchased from Sigma-Aldrich (St. Louis, MO).

2.2 QCM-D Experiments

The immobilization of B lymphoblast cells on gold surface was studied using a quartz crystal microbalance with dissipation monitoring QCM-D (Q-Sense E4, Biolin Scientific, Västra Frölunda, Sweden). Gold-coated quartz crystals i.e., sensor chips (a fundamental frequency of 5-MHz) were purchased from Biolin and used according to the manufacturer's instructions. New gold-coated sensor chips were sequentially rinsed with deionized water and absolute ethanol and then dried under a nitrogen stream. The chips were next placed in an UV/ozone chamber for 20 minutes, and incubated in base piranha solution (20 mL ammonia solution, 20 mL hydrogen peroxide in 30 mL deionized water) for 20 minutes then rinsed with deionized water, and dried under a nitrogen stream. A freshly cleaned chip was mounted into the QCM-D chamber before every experiment.

2.3 Modifications of the Chip Surface

The chip surface was modified in 2 different ways in the experiments: MPS or MUA coatings. For MPS coating the solution of 10 μL MPS, 2,34 mg KOH, 50 μL deionized water, and 10 mL ethanol at pH 9 was introduced to the chamber (60 minutes), then the sensor was rinsed with ethanol and deionized water to wash out loosely absorbed material. For the MUA coating the solution of 1 mM MUA in ethanol was introduced to the chamber until the signal is stabilized (60 minutes), then the sensor was rinsed with ethanol and deionized water to wash loosely absorbed material. For the uncoated sensor experiments (method A), phosphate buffered saline (PBS) was introduced to the chamber and the surface allowed to equilibrate in PBS (pH 7.4) until a stable first overtone frequency was observed (1 Hz over 10 minutes). This procedure was typically accomplished in 40–50 minutes.

2.3.1 Cross-Linkers

Two different cross-linkers were used in the experiments; EDC/NHS and Sulfo-SMCC. For EDC/NHS crosslinking the solution of 5 mg EDC, 5 mg NHS in 1 mL deionized water was introduced to the chamber including the sensor modified with MPS for 45 minutes. Then, the surface was rinsed with deionized water and PBS (pH 7.4) to wash out loosely absorbed material. For Sulfo-SMCC crosslinking, the solution of 1 mg Sulfo-SMCC in 1 mL deionized water was introduced to the chamber including the sensor modified with MPS for 45 minutes. Then, the sensor was rinsed with deionized water and PBS to wash out loosely absorbed material.

2.3.2 Protein G and CD19 Antibody Immobilization

The protein G solution, 800 μL protein G (5% protein G solution in deionized water) in 5.4 mL PBS was introduced to chamber for 60 minutes. Then the sensor surface was rinsed with PBS. The 500 mL of stock solution of CD19 (20 μL CD19 antibody in 1 mL PBS) was diluted in 5.4 mL PBS and then introduced to chamber until the signal was stabilized (60 minutes), followed by PBS rinsing.

2.3.3 BSA Blocking

The solution, 5% BSA solution (0.5 mg BSA in 10 mL PBS) was introduced to the chamber to prevent non-specific binding of cells for 45 minutes, followed by PBS rinsing.

2.3.4 Capturing B Lymphoblast Cells

For determining the optimum surface functionalization method, 10^4 cells/mL of B lymphoblast cells in PBS were introduced into flow chamber for 60 minutes. After determining the surface functionalization method, solu-

tion containing 10^3, 10^4, 10^6 B lymphoblast cells per mL in PBS were introduced into flow chamber containing the functionalized sensor for 60 minutes to determine the concentration dependency. Prior cell count was performed both with Muse Cell Analyzer (Merck, Billerica MA) device and manually with a Neubauer Chamber.

Each experiment was repeated at least 3 times to obtain the means and standard deviations of the frequency shift data, the error bars indicate the standard deviation from the average values. Statistical significance was considered at $P < 0.05$. Student's t-test was performed for the experimental results.

3 Results and Discussion

Method A: Adsorption and covalent bonding are widely used techniques to immobilize receptors on surfaces. Adsorption is practical and has been demonstrated for various sensors [5,23]. The adsorption mechanism of protein G on gold surface was analyzed by Johnson and Mutharasan [58]; in our work, the solution of protein G at pH of 7.4 caused an average frequency shift of 10.7 Hz due to the adsorption on the bare gold surface (Figure 2).

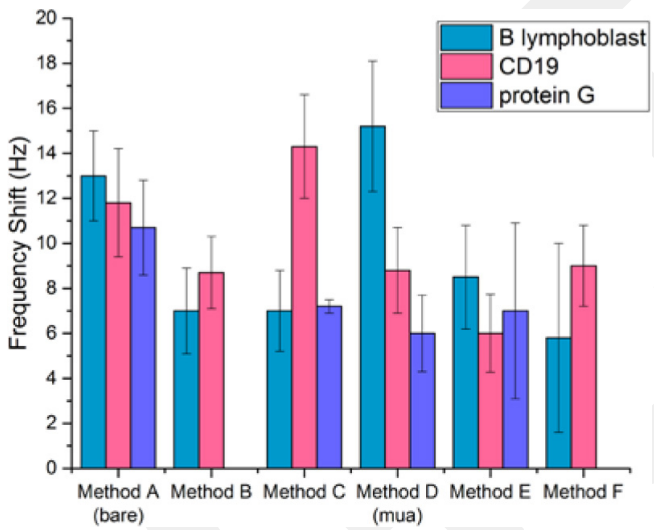

Fig. 2. The QCM frequency shifts for B lymphoblast, CD19 antibody and protein G for all methods. Error bars indicate the standard deviation from the average values. For the frequency shifts of B lymphoblast cells, $P < 0.05$ between the method D and methods (B, C, E, F). $P > 0.05$ between the method D and method A.

Methods B and C are based on MPS coating of the gold surface and forming the Sulfo-SMCC bifunctional cross-linker for protein immobilization. The hydrolyzed MPS self-assembled monolayer results in laterally condensed –OH groups and upright non-condensed OH groups on gold surface [60]. The maleimide of the Sulfo-SMCC reacting with the sulfhydryl placed vertically on the sensor surface forms an inclined crosslink with the 120° angle [61]. The NHS-ester in the Sulfo-SMCC reacts with the amine of the protein [62]. We tried both protein G and CD19 antibody on the Sulfo-SMCC linker but the cell capture ratio was lower compared to other methods. This can be due to the 120° angled bond between the maleimide on Sulfo-SMCC and the upright thiols on the sensor surface, and also lack of MPS lamination results in fewer thiol groups on the surface [63]. The average frequency shift for Sulfo-SMCC layer on MPS was 3.96 Hz that is lower compared to the average frequency shifts for EDC/NHS layer on MUA and MPS (9.58 Hz and 9.46 Hz, respectively). Even though the frequency shifts for CD19 and protein G indicate surface binding, the low frequency shift for cell capture suggests that the protein G and CD19 antibody are not orientated on the Sulfo-SMCC layer for efficient cell capture (Figure 2).

Method D is based on covalent bond between gold and sulfur in MUA and EDC/NHS bifunctional linker for protein immobilization. The sulphide-based MUA self-assembled monolayer results in –COOH groups on gold. The EDC-NHS crosslinking forms succinimide groups on gold surface for protein binding [59].

Method E is the combination of MPS coating of gold and EDC/NHS crosslinking. Typically, EDC/Sulfo-NHS protocol has been used to functionalize hydroxyl groups as Amine reactive. The Hydroxyl ions independent from Carboxyl groups are capable of reacting with electrophilic carbodiimides via the nucleophilic effect of hydroxyl ions. Thus, the hydroxyl groups independent from Carboxyl groups on MPS coating could be functionalized as Amine reactive by using EDC/Sulfo-NHS protocol [64].

Method D has higher cell capture ratio compared to Method E, though even though the protein G binding is lower. By monitoring the resonance frequency shifts, which were due to the Protein G binding onto the both surfaces coated with MPS and MUA, a real time measurement of Protein G amount on the sensor surface with respect to time was obtained. By using Equation 1, the quantity of Protein G on the sensor surface coated with MPS (9.7 Hz frequency shift) was calculated approximately as 25 of Protein G per 500 nm^2 of area, and the quantity of Protein G on the sensor surface coated with MUA (5.6 Hz frequency shift) was calculated approximately as 14 of Protein G per 500 nm^2 of area. To validate the QCM measurements, Atomic Force Microscopy (AFM, Veeco Multimode 8) was used to determine the quantity of Protein G for MPS and MUA coatings as well as to examine the surface morphology of both coatings (Figure 3).

The condensation of MPS in aqueous ethanol solution at high pH provides that the functionalized sensor surface is more compact than the coating with non-condensed MUA [36]. In the study of Oh *et al.*, it was reported that Protein G molecules in a solution form cloud-like structures, and they are adsorbed onto a bare Au surface as a clustered pattern [65]. As seen in Figure 3, AFM measurement reveals that protein G layer is more uniform and dense on MPS layer compared to MUA layerm and QCM measurements confirms that protein G layer has

higher binding on MPS surface for the method E. When the calculations with Sauerbrey Equation and AFM analysis are considered, it can be proved that more Protein G on the MPS coated surface is preserved, and MPS coating is more compact.

In order to investigate the impact of Protein G to cell capture, the experiments without Protein G (method F) was performed resulting in the lowest cell capture ratio. Protein G provides appropriate antibody orientation and thus higher cell capture ratio. Higher CD19 antibody binding to the surface did not result in higher cell capture ratio due to the random orientation of the antibody thus decreased cell binding efficiency.

Even though MPS coated surface has higher binding for protein G, the cell capture ratio is lower. To understand the impact of BSA passivation layer, method D and method E were performed without introducing BSA. Eliminating BSA in Method D did not result in any significant difference. However, eliminating BSA layer in Method E increased the cell capture ratio (Figure 4).

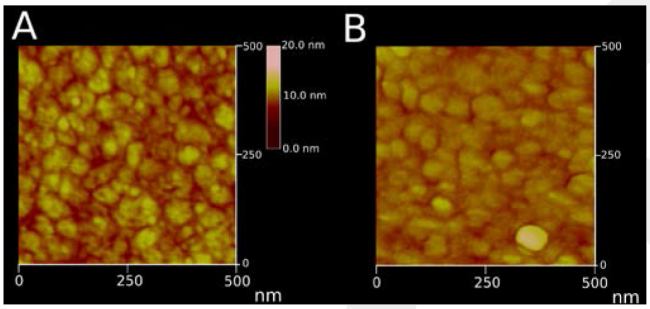

Fig. 3. The AFM analysis of the protein G layer on A) MPS and B) MUA coatings.

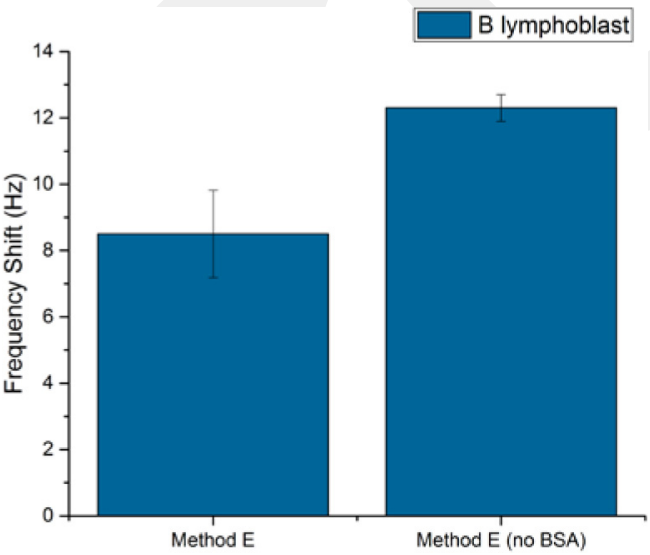

Fig. 4. The QCM frequency shifts for B lymphoblast, CD19 antibody and protein G for the method E with and without BSA. Error bars indicate the standard deviation from the average values; $P < 0.05$ between the method E and method E (no BSA).

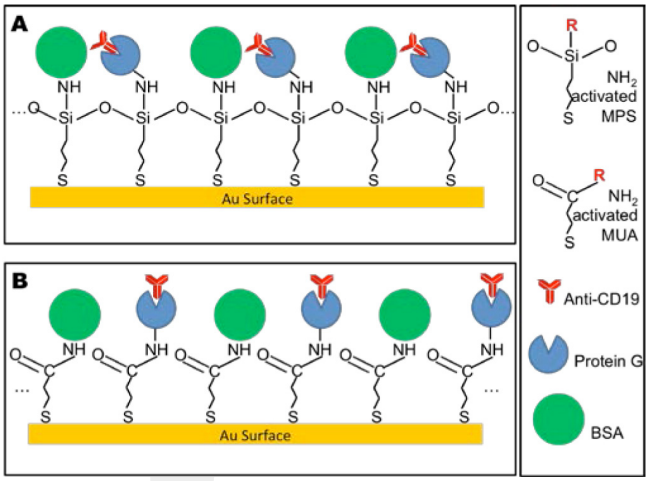

Fig. 5. The schematic illustrations of surface functionalization and the impact of BSA blocking A) MPS B) MUA.

As Protein G's surface coverage depends on the quantity of amine-reactive groups on the sensor surface its orientation also depends on another critical parameter, pH. At pH = 7.4, which is the same with the Phosphate Buffered Saline (PBS) used as a buffer solution in this study, the immobilized protein G's active sites (Glu27, Lys28, Lys31, Gln32, and Asn35) concerning with the heavy chain sites of IgG (Fc) directs upward due to the neutral electrostatic effect of medium's pH [40,58].

As illustrated in Figure 5, Protein G on the MUA coated Au surface directs upward because of the bonding angle of amine with Sulfo-NHS [66]. On the other hand, Protein G on the MPS coated Au surface makes inclined bonding with the amine reactive groups, and this angled bonding causes the sloping direction of Protein G.

After BSA blocking, which is used to prevent non-specific binding, BSA is more likely to hinder the antibody to engage the target cell. Because of the hindrance of BSAs on the sensor surface and the angle of protein Gs, the resonance frequency shift caused by target cell capturing with the MPS coated sensor is lower when compared with the resonance frequency shift for the system coated with MUA. The impact of BSA blocking also investigated by AFM measurements (Figure 6). In Figure 6A, the BSA on the MPS layer is similar to the one as illustrated in Figure 5A where BSA molecules created a more compact surface. The more compact sensor surface having more amine reactive groups as in Method E naturally have more BSA attached on the surface. The dense layer of BSA molecules with dimensions 4 nm × 4 nm × 14 nm [67] inhibits the inclined IgGs on the MPS coating with dimensions 4 nm × 8.5 nm × 14.5 nm as in explained in Figure 5. Conversely, it is expected that the hindrance effect of quantitatively fewer BSA molecules on MUA coating on the IgGs uprightly placed the sensor surface is much less. This less hindrance effect on the IgGs on MUA coating provides the IgGs to capture the target cells readily.

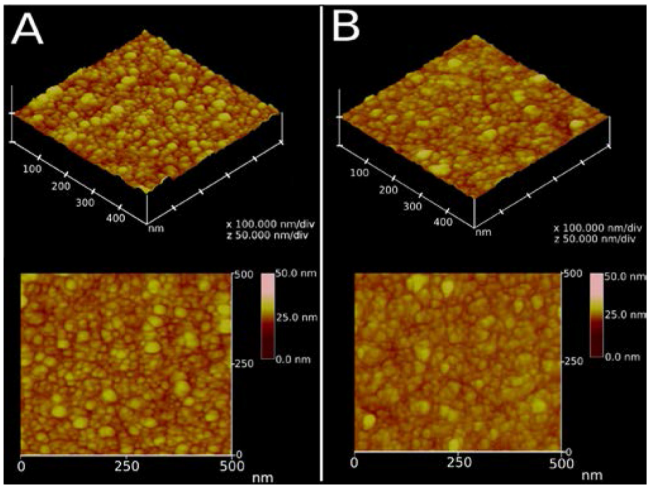

Fig. 6. The AFM analysis of the BSA layer on A) MPS and B) MUA coatings.

Even though MPS coating results in a uniform protein G layer on the sensor surface, the BSA layer on MPS and pH reduces the cell binding. Also MPS is pH, coating repetition and time sensitive that makes it difficult to control the surface uniformity [36].

Due to the disadvantages of MPS coating and in the light of the QCM measurements, method D that includes MUA coating, EDC/NHS cross-linking, protein G, CD19 antibody and BSA passivation was determined as the optimum method for surface functionalization to capture B lymphoblast cells. In order to visualize the cells on functionalized gold surfaces, the method D was applied to gold-coated surfaces for bright field optical micrographs (Figure 7).

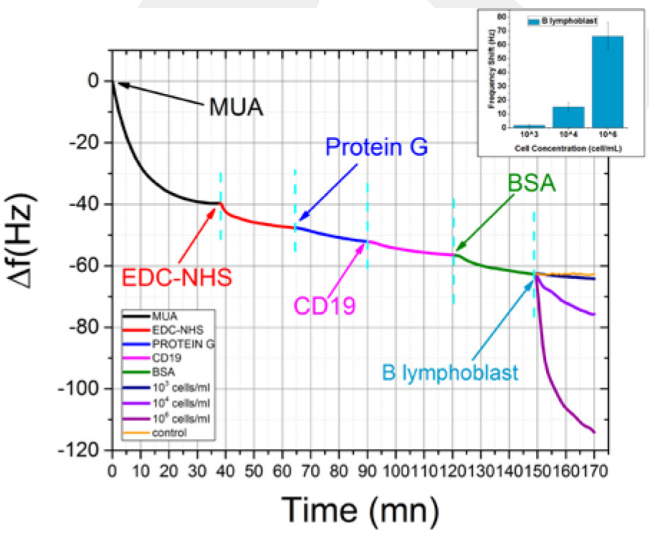

Fig. 8. QCM frequency shifts for the main steps of the method D and concentration dependency. Error bars indicate the standard deviation from the average values; $P < 0.05$ between the concentration pairs of 10^3 and 10^4, 10^3 and 10^6, 10^4 and 10^6 cell/mL.

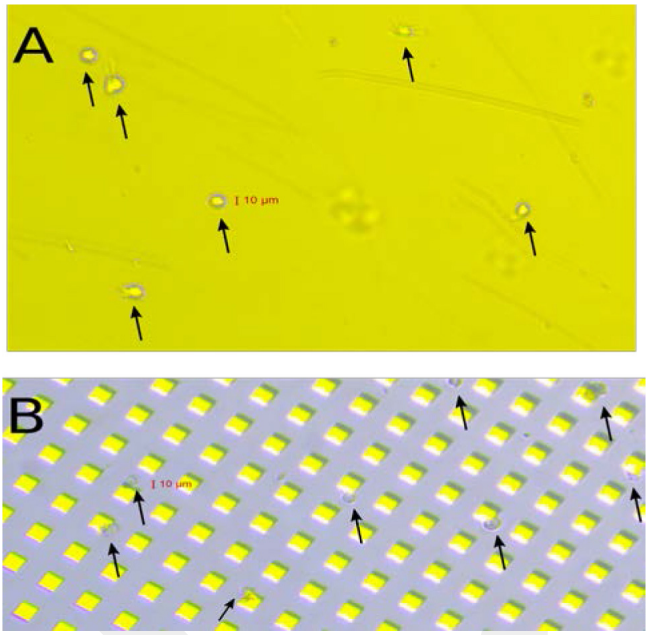

Fig. 7. Bright-Field Optical Micrographs of the cells captured on modified gold surfaces: A) Planar gold surface, B) Square gold surface on glass. Black arrows indicate the cells captured on the surface.

Figure 7A shows a QCM sensor surface and Figure 7B shows square shaped gold pads on a glass substrate. The black arrows indicate the captured cells on the surface.

The method D was also tested by changing the concentration of the B lymphoblast cells (Figure 8). Injection of 10^3, 10^4 and 10^6 cells per mL to the QCM chamber resulted in 1.9 Hz, 15.2 Hz and 66.2 Hz frequency shift, respectively. The QCM frequency response was also consistent with the dose increment.

4 Conclusion

Our goal is to develop a biochip to capture B lymphoblast cells on the gold-coated sensor surface and quantify the cells. In order to capture B lymphoblast cells, the gold surfaces can be functionalized with CD19 antibody as recognition elements. As a first step towards the biochip, an immobilization technique for the CD19 antibody has to be determined. Here, we report the QCM results of various surface modification strategies to immobilize CD19 antibody on gold surface and capture B lymphoblast cells. The protein G has significant impact on cell capture efficiency. Even though higher amount of CD19 antibody bind to surface in method F, higher cell capture ratio measured for method E is due to the protein G presence and orientation of the CD19 antibody. MPS and Sulfo-SMCC combination did not result in high cell capture ratios for QCM as multiple layers of MPS required to increase the Sulfo-SMCC binding. It was also validated that protein G has affinity to bare gold surface (method A). Self assembled monolayer of MUA followed

by EDC/NHS activation has been used for antibody immobilization, and the CD19 immobilization resulted in higher cell capture when used together with protein G. The unprecedented MPS-EDC/NHS method has also advantages for biosensors to enable a smoother sensor surface and more homogeneous receptor dispersion on the surface, but BSA blocking and pH dependency reduce the cell binding ratios. In the case of MPS-EDC/NHS combination, another blocking agent other than BSA should be tested. For these reasons, MUA ≫ EDC/NHC ≫ protein G ≫ CD19 antibody ≫ BSA layers are preferred to capture B lymphoblast cells. After determining the optimum method, we performed concentration experiments. The QCM sensor surface was functionalized using the optimum method and different cell concentrations were introduced to QCM chamber. Minimum 10^3 cell per mL was measured as 1.9 Hz frequency shift whereas 10^6 cell per mL was measured as 66.2 Hz frequency shift. Our next efforts will be to apply and optimize the preferred immobilization procedure for gold surfaces in a microfluidic platform. As an alternative to the method D, method A can be also preferred for surface functionalization. Method D provided higher cell capture ratio, and the statistical test result suggests method A is not significantly different from method D. For long-term stability covalent binding provides stronger bonds compared to surface adsorption thus method D was chosen as the optimum method.

Acknowledgements

Authors acknowledge The Scientific and Technological Research Council of Turkey (TÜBİTAK Project No: 115E020) for financial support and Prof. Servet Ozcan and Prof. Musa Karakukcu from Erciyes University for valuable discussions for the cell line related issues. Authors also acknowledge Tayyibe Gercek for growing cell cultures and Furkan Soysaldi for helping on preparation of QCM data.

References

[1] M. Hauwel, T. Matthes, *Swiss Med. Wkly.* **2014**, *144*, DOI 10.4414/smw.2014.13907.
[2] J. J. M. van Dongen, V. H. J. van der Velden, M. Brüggemann, A. Orfao, *Blood* **2015**, *125*, 3996–4009.
[3] G. Gaipa, G. Basso, A. Biondi, D. Campana, *Cytometry Part B* **2013**, *84*, 359–369.
[4] P. Vadgama, P. W. Crump, *Analyst* **1992**, *117*, 1657.
[5] K. Icoz, C. Savran, *Appl. Phys. Lett.* **2010**, *97*, 123701.
[6] B. Dhayal, W. A. Henne, D. D. Doorneweerd, R. G. Reifenberger, P. S. Low, *J. Am. Chem. Soc.* **2006**, *128*, 3716–3721.
[7] P. S. Waggoner, H. G. Craighead, *Lab Chip* **2007**, *7*, 1238–1255.
[8] G. Zheng, C. M. Lieber, *Methods Mol. Biol.* **2011**, *790*, 223–237.
[9] G. J. Zhang, Y. Ning, *Anal. Chim. Acta* **2012**, *749*, 1–15.
[10] P. Namdari, H. Daraee, A. Eatemadi, *Nanoscale Res. Lett.* **2016**, *11*, 406.
[11] J. Zhang, Y. Sun, B. Xu, H. Zhang, Y. Gao, H. Zhang, D. Song, *Biosens. Bioelectron.* **2013**, *45*, 230–236.
[12] H. Šípová, J. Homola, *Anal. Chim. Acta* **2013**, *773*, 9–23.
[13] P. Singh, *Sens. Actuators B* **2016**, *229*, 110–130.
[14] M. Varshney, Y. Li, *Biosens. Bioelectron.* **2009**, *24*, 2951–2960.
[15] A. T. Sage, J. D. Besant, B. Lam, E. H. Sargent, S. O. Kelley, *Acc. Chem. Res.* **2014**, *47*, 2417–2425.
[16] J. Liu, S. Wagan, M. Dávila Morris, J. Taylor, R. J. White, *Anal. Chem.* **2014**, *86*, 11417–11424.
[17] R. A. Sperling, P. Rivera Gil, F. Zhang, M. Zanella, W. J. Parak, *Chem. Soc. Rev.* **2008**, *37*, 1896.
[18] P. D. Howes, R. Chandrawati, M. M. Stevens, *Science (80-.).* **2014**, *346*, 1247390-1-1247390–10.
[19] E. Hutter, D. Maysinger, *Trends Pharmacol. Sci.* **2013**, *34*, 497–507.
[20] M. S. Szymanski, R. A. Porter, *J. Immunol. Methods* **2013**, *387*, 262–269.
[21] S. Nantaphol, O. Chailapakul, W. Siangproh, *Anal. Chim. Acta* **2015**, *891*, 136–143.
[22] A. Abbaspour, F. Norouz-Sarvestani, A. Noori, N. Soltani, *Biosens. Bioelectron.* **2015**, *68*, 149–155.
[23] K. İçöz, O. Mzava, *Appl. Sci.* **2016**, *6*, 394.
[24] J. Y. Hou, T. C. Liu, G. F. Lin, Z. X. Li, L. P. Zou, M. Li, Y. S. Wu, *Anal. Chim. Acta* **2012**, *734*, 93–98.
[25] M. C. Lim, G. H. Lee, D. T. N. Huynh, C. E. Hong, S. Y. Park, J. Y. Jung, C. S. Park, S. Ko, Y. R. Kim, *Colloids Surf. B* **2016**, *145*, 854–861.
[26] I. H. Cho, L. Mauer, J. Irudayaraj, *Biosens. Bioelectron.* **2014**, *57*, 143–148.
[27] Y. Alapan, K. Icoz, U. A. Gurkan, *Biotechnol. Adv.* **2015**, *33*, 1727–1743.
[28] S. K. Vashist, E. Lam, S. Hrapovic, K. B. Male, J. H. T. Luong, *Chem. Rev.* **2014**, *114*, 11083–11130.
[29] M. Singh, M. Holzinger, M. Tabrizian, S. Winters, N. C. Berner, S. Cosnier, G. S. Duesberg, *J. Am. Chem. Soc.* **2015**, *137*, 2800–2803.
[30] S. Jiang, K. Y. Win, S. Liu, C. P. Teng, Y. Zheng, M.-Y. Han, *Nanoscale* **2013**, *5*, 3127–48.
[31] R. A. Bohara, N. D. Thorat, S. H. Pawar, *RSC Adv.* **2016**, *6*, 43989–44012.
[32] V. Biju, *Chem. Soc. Rev.* **2014**, *43*, 744–764.
[33] F. Frederix, K. Bonroy, W. Laureyn, G. Reekmans, A. Campitelli, W. Dehaen, G. Maes, **2003**, DOI 10.1021/LA026908F.
[34] M. G. Kim, Y. B. Shin, J. M. Jung, H. S. Ro, B. H. Chung, *J. Immunol. Methods* **2005**, *297*, 125–132.
[35] A. Kausaite-Minkstimiene, A. Ramanaviciene, A. Ramanavicius, *Analyst* **2009**, *134*, 2051–2057.
[36] M. C. Soylu, W.-H. Shih, W. Y. Shih, *Ind. Eng. Chem. Res.* **2013**, *52*, 2590–2597.
[37] C. Zhou, J.-M. Friedt, A. Angelova, K.-H. Choi, W. Laureyn, F. Frederix, L. A. Francis, A. Campitelli, Y. Engelborghs, G. Borghs, *Langmuir* **2004**, *20*, 5870–5878.
[38] J. Baniukevic, J. Kirlyte, A. Ramanavicius, A. Ramanaviciene, *Sens. Actuators B* **2013**, *189*, 217–223.
[39] A. Makaraviciute, A. Ramanaviciene, *Biosens. Bioelectron.* **2013**, *50*, 460–471.
[40] A. E. Sauer-Eriksson, G. J. Kleywegt, M. Uhlén, T. A. Jones, *Structure* **1995**, *3*, 265–278.
[41] H. Y. Song, X. Zhou, J. Hobley, X. Su, *Langmuir* **2012**, *28*, 997–1004.
[42] C. Kößlinger, S. Drost, F. Aberl, H. Wolf, S. Koch, P. Woias, *Biosens. Bioelectron.* **1992**, *7*, 397–404.
[43] G. G. Guilbault, B. Hock, R. Schimid, *Biosens. Bioelectron.* **1992**, *7*, 411–419.

[44] S. Babacan, P. Pivarnik, S. Letcher, A. G. Rand, *Biosens. Bioelectron.* **2000**, *15*, 615–621.
[45] P. Abdul Rasheed, N. Sandhyarani, *Anal. Chim. Acta* **2016**, *905*, 134–139.
[46] X. Li, S. Song, Y. Pei, H. Dong, T. Aastrup, Z. Pei, *Sens. Actuators B* **2016**, *224*, 814–822.
[47] N. A. Masdor, Z. Altintas, I.E. Tothill, *Biosens. Bioelectron.* **2016**, *78*, 328–336.
[48] T. M. Clausen, M. A. Pereira, H. Z. Oo, M. Resende, T. Gustavson, Y. Mao, N. Sugiura, J. Liew, L. Fazli, T. G. Theander, et al., *Sens. Bio-Sensing Res.* **2016**, *9*, 23–30.
[49] C. Kößlinger, S. Drost, F. Aberl, H. Wolf, *Fresenius J. Anal. Chem.* **1994**, *349*, 349–354.
[50] J. E. Roederer, G. J. Bastiaans, *Anal. Chem.* **1983**, *55*, 2333–2336.
[51] H. Muramatsu, J. M. Dicks, E. Tamiya, I. Karube, *Anal. Chem.* **1987**, *59*, 2760–2763.
[52] M. Muratsugu, H. Ikeda, F. Ohta, Y. Miya, T. Hosokawa, S. Kurosawa, N. Kamo, *Anal. Chem.* **1993**, *65*, 2933–2937.
[53] K. Nakanishi, H. Muguruma, I. Karube, *Anal. Chem.* **1996**, *68*, 1695–1700.
[54] M. C. Dixon, *J. Biomol. Tech.* **2008**, *19*, 151–158.
[55] A. Wargenau, N. Tufenkji, *Anal. Chem.* **2014**, *86*, 8017–8020.
[56] G. Sauerbrey, *Zeitschrift fuer Phys.* **1959**, *155*, 206–222.
[57] A. Karczmarczyk, K. Haupt, K. H. Feller, *Talanta* **2017**, *166*, 193–197.
[58] B. N. Johnson, R. Mutharasan, *Langmuir* **2012**, *28*, 6928–34.
[59] F. Inci, C. Filippini, M. Baday, M. O. Ozen, S. Calamak, N. G. Durmus, S. Wang, E. Hanhauser, K. S. Hobbs, F. Juillard, et al., *Proc. Natl. Acad. Sci. USA* **2015**, *112*, E4354-63.
[60] I. Byun, A. W. Coleman, B. Kim, *J. Micromech. Microeng.* **2013**, *23*, 85016.
[61] C. Walther, K. Meyer, R. Rennert, I. Neundorf, *Bioconjugate Chem.* **2008**, *19*, 2346–2356.
[62] J. A. Capobianco, W. Y. Shih, W. H. Shih, *Rev. Sci. Instrum.* **2007**, *78*, DOI 10.1063/1.2727466.
[63] W. Wu, W.-H. Shih, W. Y. Shih, *J. Appl. Phys.* **2016**, *119*, 124512.
[64] R. S. Banegas, C. F. Zornio, A. de M. G. Borges, L. C. Porto, V. Soldi, *Polímeros* **2013**, *23*, 182–188.
[65] B. K. Oh, W. Lee, Y. K. Kim, W. H. Lee, J. W. Choi, *J. Biotechnol.* **2004**, *111*, 1–8.
[66] J. Bart, R. Tiggelaar, M. Yang, S. Schlautmann, H. Zuilhof, H. Gardeniers, *Lab Chip* **2009**, *9*, 3481–3488.
[67] S. J. McClellan, E. I. Franses, *Colloids Surf. A* **2005**, *260*, 265–275.

Received: December 1, 2017
Accepted: January 20, 2018
Published online on ■■, ■■■

FULL PAPER

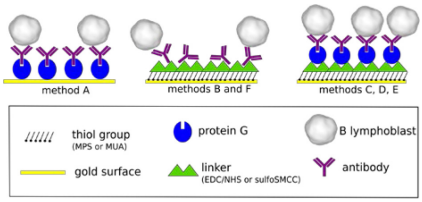

K. Icoz, M. C. Soylu, Z. Canikara, E. Unal*